Open access • Journal Article • DOI:10.1007/S00259-019-04369-6

[11C]JNJ54173717, a novel P2X7 receptor radioligand as marker for neuroinflammation: human biodistribution, dosimetry, brain kinetic modelling and quantification of brain P2X7 receptors in patients with Parkinson's disease and healthy volunteers. — Source link

Donatienne Van Weehaeghe, Michel Koole, Mark E. Schmidt, Stephanie Deman ...+7 more authors

Institutions: Katholieke Universiteit Leuven, Janssen Pharmaceutica, European Institute

Published on: 26 Jun 2019 - European Journal of Nuclear Medicine and Molecular Imaging (Eur J Nucl Med Mol Imaging)

[^{11}C]JNJ54173717, a novel P2X7 receptor radioligand as marker for neuroinflammation: human biodistribution, dosimetry, brain kinetic modelling and quantification of brain P2X7 receptors in patients with Parkinson's disease and healthy volunteers.

Donatienne Van Weehaeghe[1], Michel Koole[1], Mark E. Schmidt[2], Stephanie Deman[3], Andreas H. Jacobs[4], Erika Souche[3,], Kim Serdons[1], Stefan Sunaert[5], Guy Bormans[6], Wim Vandenberghe[7,8], Koen Van Laere[1]

[1] Division of Nuclear Medicine and Molecular Imaging, University Hospitals of Leuven and KU Leuven, Belgium

[2] Janssen Research and Development: Beerse, Belgium

[3] Genomics Core, UZ Leuven, and Department of Human Genetics, KU Leuven, Leuven, Belgium

[4] European Institute for Molecular Imaging (EIMI), Westfalian Wilhelms University (WWU) Münster, and Department of Geriatrics and Neurology, Johanniter Hospital Bonn, Germany

[5]Department of Radiology, University Hospitals Leuven, Gasthuisberg, UZ, Leuven, Belgium

[6] Laboratory for Radiopharmaceutical Research, KU Leuven, Belgium

[7]Department of Neurosciences, KU Leuven, Leuven, Belgium

[8]Department of Neurology, University Hospitals Leuven, Belgium

CORRESPONDING AUTHOR

Donatienne Van Weehaeghe, MD

donatienne.vanweehaeghe@uzleuven.be

Tel +32 16 34 37 15

Fax +32 16 34 37 59

ACKNOWLEDGEMENTS

The authors explicitly want to thank Mr. Kwinten Porters and Mr. Jef Van Loock for their contributions to the scanning and data handling, the PET radiopharmacy team, the medical physics team of UZ Leuven for their skilled contributions and the Michael J Fox foundation for their financial support (PRI-PD project, Grant ID 12062).

ABSTRACT

Purpose

The P2X7 receptor (P2X7R) is an ATP-gated ion channel predominantly expressed on activated microglia which is important in neurodegenerative diseases including Parkinson's disease (PD). In this first-in-human study we investigated [^{11}C]JNJ54173717 ([^{11}C]JNJ717), a selective P2X7R tracer, in healthy volunteers (HV) and PD patients. Biodistribution, dosimetry, kinetic modelling and short-term test-retest variability (TRV), as well as possible genotype effects were investigated.

Methods

Biodistribution and radiation dosimetry studies were performed in 3 HV (30 ± 2 y, 2F) using whole body PET-CT. Using 90-min dynamic simultaneous PET-MR scans in 11 HV (62 ± 10 y, 6F) and 10 PD patients (64 ± 8 y, 3F, UPDRS motor score 21 ± 8), the most appropriate kinetic model was determined. The total volume of distribution (V_T) was calculated using a 1- and 2-tissue compartment model (1-2TCM) and Logan graphical analysis and its time stability was assessed. Seven subjects underwent retest scans (60 ± 13 y, 4HV, 1F). A group analysis was performed to compare PD with HV. Finally, 13 exons of P2X7R were genotyped in all subjects from part two.

Results

The effective dose was 4.47 ± 0.32 µSv/MBq, with highest absorbed doses for gallbladder, liver and small intestine. A reversible 2TCM was the most appropriate kinetic model with relatively homogeneous V_T values in grey and white matter. Average V_T was 3.4 ± 0.8 for HV and 3.3 ± 0.7 for PD, without significant group differences, but a possible genotype effect (rs3751143) was identified which can affect V_T. Average TRV was 10-15%. Time stability allowed reduction of scan time to 70 minutes.

Conclusion

[^{11}C]JNJ717 is safe and suitable for quantifying P2X7R expression in human brain. In this pilot study, no significant differences in P2X7R binding were found between HV and PD. Moreover, our results suggest genotype effects need to be incorporated in future P2X7R PET analyses.

Keywords: P2X7 receptor, neuroinflammation PET, Parkinson, dosimetry, genotyping, [^{11}C]JNJ54173717

INTRODUCTION

Activated microglia are a hallmark of neuroinflammation and are thought to play a central role in pathogenesis and progression of neurodegenerative diseases such as Parkinson's disease (PD), Alzheimer's disease (AD) and Amyotrophic Lateral Sclerosis (ALS) [1]. The purinergic P2X7 receptor (P2X7R), an adenosine triphosphate (ATP)-gated ion channel, is expressed mainly on activated microglia throughout the brain and spinal cord [2, 3]. However, low P2X7R expression is also present on neurons, astrocytes and oligodendrocytes as still 17% of the P2X7R mRNA signal remained in hippocampal slice cultures depleted of microglia [4]. Stimulation of P2X7R initiates the release of pro-inflammatory cytokines such as IL-1ß and IL-18 by promoting the NLPR3 inflammasome assembly [5]. Furthermore, preclinical data in an AD mice model have shown that P2X7R antagonism reduced formation of hippocampal amyloid plaques, resulting in reduced cognitive impairment and improved dendritic spine development [6, 7]. In a PD rat model, P2X7R antagonism increased tyrosine hydroxylase immunoreactivity and decreased loss of nigral dopaminergic neurons such that hemiparkinsonism was partially reverted [8, 9]. In an ALS mice model, motor coordination was improved by P2X7R antagonism while weight loss was delayed and survival increased [10]. On the other hand, in P2X7R knockout mice with toxin-induced parkinsonism no neuroprotective effect was observed [11]. Moreover, an exacerbation of pathology was demonstrated in ALS mice models [12]. Also post-mortem, the importance of P2X7R was illustrated as an increased (about twofold) P2X7R immunoreactivity was observed in the spinal cord in ALS and Multiple Sclerosis patients compared to controls, although the cause of death was not taken into account in this study as potential confounder [13].

Accordingly, in-vivo visualisation and quantification of P2X7R in the brain is of great importance to study pathogenesis in human neurodegenerative disorders and to allow therapeutic drug monitoring. Recently, a fluorine-18 P2X7R compound ([^{18}F]JNJ64413739) with acceptable test-retest variability (± 10%) for a 90 minutes acquisition protocol was developed. However, a carbon-11 compound can be beneficial as it facilitates one day scan protocols such as dose occupancy studies. In collaboration with Janssen Pharmaceuticals, a promising ^{11}C-P2X7R radiotracer [^{11}C]JNJ54173717 ([^{11}C]JNJ717) was developed showing a nanomolar affinity for human P2X7R (K_D = 1.6 nM). Selectivity and kinetics of [^{11}C]JNJ717 were investigated in a rat model with local brain lentiviral overexpression of human P2X7R and in monkeys showing negligible nonspecific binding and good blood-brain barrier permeability [14].

In this first-in-human study we report biodistribution, dosimetry, kinetic modelling and short-term test-retest variability (TRV) of [^{11}C]JNJ717 in a set of healthy volunteers (HV) and PD patients. Secondly, we investigated

group differences between 10 PD patients and 11 age-matched HV with regard to P2X7R distribution and structural changes. Furthermore, we examined a possible genotype effect on binding affinity or expression level as the human P2X7R is highly polymorphic [15].

MATERIALS AND METHODS

Study design and objectives

HV were recruited in response to advertisements on the internet and departmental websites. The main exclusion criteria included: abnormal physical or neurological examination or paraclinical investigations, history of significant medical illnesses including major internal pathology or neurological and neuropsychiatric disorders, history of clinically relevant drug or food allergies, and use of chronic - or acute if shortly for scan - anti-inflammatory medication such as non-steroidal antiphlogistics and systemic corticosteroids. Inclusion criteria for PD patients were: older than 45 years and diagnosis of PD according to UK brain bank criteria with at least two main symptoms (resting tremor, bradykinesia or rigidity). In total 14 HV and 10 PD patients were included for the two study parts. In the first part dosimetry was assessed, in the second part kinetic modelling, test-retest variability (TRV) and group comparisons. For each study part, demographic data and tracer information are summarized in Table 1. Short-term test-retest scans were conducted in 4 HV and 3 PD patients. PD patients were clinically characterized using UPDRS part 3 (motor score) and Hoehn-Yahr scale on medication. Levodopa-equivalent daily dose (LED) was calculated as described previously [16]. The study was approved by the local Ethics Committee (Ethical Committee UZ/KU Leuven) and performed in accordance to the World Medical Association Declaration of Helsinki. Written informed consent was obtained from all the subjects prior to the study.

Biodistribution and dosimetry studies

The biodistribution and dosimetry study was performed in 3 young HV (30 ± 2 y, 1M/2F) by consecutive whole body (WB) PET-CT scanning from the midfemoral position to the head (nine sequential WB scans from tracer injection to 90 min post injection). The mean injected activity was 189 ± 43 MBq with a mean specific (molar) activity of 109 ± 83 GBq/µmol.

The WB PET-CT scans were executed on a Hirez Biograph 16 PET-CT camera (Siemens, Ehrlangen, Germany). A vacuum cushion and body strap were used to limit motion during scanning. Data were corrected for randoms, scatter and attenuation and reconstructed using 3D OSEM (Ordered Subset Expectation Maximization) iterative reconstruction (5 iterations and 8 subsets) with correction followed by a Gaussian postsmoothing with a 6 mm Full Width Half Maximum (FWHM). For attenuation correction a low dose CT scan prior to PET scanning was performed.

Normalized Cumulated Activities values (NCA) were calculated by dividing the area under the time activity curves (TAC) of each source organ by the total injected activity. For the small intestine, upper and lower large intestine the ICRP 30 gastrointestinal model was used. The fraction entering the small intestine was used as input and set equal to the decay-corrected plateau fraction of injected activity encompassed by the intestinal VOI. Based on the NCA values, absorbed doses were calculated using OLINDA v1.1 [17], according to ICRP 60 [18] definition and using the Medical Internal Radiation Dose scheme. The Effective Dose (ED) was calculated from the individual organs doses based on predefined organ weighting factors, as specified by ICRP 60 [18].

Tracer kinetic modelling, test-retest variability and group comparisons

Eleven HV (62 ± 10 y, 6F) and 10 PD patients (64 ± 8 y, 3F, UPDRS 33 ± 12, H&Y1 [n=6] H&Y2 [n=4]) underwent a 90-minutes dynamic simultaneous PET-MR scan combined with manual arterial blood sampling and tracer radiometabolite analysis. All PD patients were on their routinely dopaminergic medication in the "ON" state. A retest scan was acquired for 7 of the 21 subjects (60 ± 13 y, 2F, 4HV, interscan interval 9 ± 13 days, range 0-28 days). The mean injected activity was 243 ± 54 MBq with a mean specific (molar) activity of 108 ± 69 GBq/µmol.

Data acquisition

PET data was acquired on a General Electric Signa PET-MR system in list mode. Images were reconstructed in 26 frames (4x15sec, 4x60sec, 2x2.5min, 16x5min) with correction for deadtime, randoms, scatter and attenuation. Attenuation correction was performed using a validated Zero Echo Time (ZTE) based approach [19]. Reconstructions were performed using 3D OSEM (28 subsets and 4 iterations), including Time of Flight (TOF) information, resolution modelling and an in-plane Gaussian postsmoothing with a 4 mm FWHM. Motion correction was executed using a frame by frame approach and a rigid co-registration of each frame with the average of the first 10 frames (first 10 min of the PET acquisition). Twenty-two arterial blood samples to calculate plasma and blood activity curves and 6 additional arterial blood samples were taken to determine the fraction of parent tracer in arterial plasma and to calculate plasma to whole blood activity ratios. The activity as determined by gamma counting of High Pressure Liquid Chromatography fractions of the metabolite analysis of plasma samples obtained at 40 and 60 minutes postinjection, showed high standard errors (13.7 ± 5.9% and 48.4 ± 210.3%, respectively). Therefore, all results are given both with individual and average metabolite corrected input curves.

Blood and plasma activity values were fitted with a three-exponential model curve while the plasma metabolite data was fitted with a sigmoid function using Pmod (v3.7, PMOD technologies, Zurich, Switzerland).

Simultaneous with PET acquisition, several MR sequences were acquired. A 3D volumetric T1-weighted BRAVO sequence (oblique plane; TE: 3.2ms; TR: 8.5ms; TI: 450ms; Flip Angle: 12; Receiver Bandwidth: 31.2; NEX: 1) and 3D T2-weigthed CUBE FLAIR sequence (oblique plane; TE: 136ms; #echoes: 1; echo train length: 190; TR: 8500ms; TI: 50ms; Receiver Bandwidth: 31.25; NEX: 1) were used.

Data analysis

Composite cortical regions were defined from the N30R83 Hammers atlas in PMOD (v3.7, PMOD technologies, Zurich, Switzerland) to delineate frontal, temporal, parietal and occipital cortical volumes of interest (VOIs) (with all cortical regions together constituting a full composite cortical VOI) as well as the cerebellum, striatum, thalamus, hippocampus and corpus callosum [20]. Left and right VOIs were grouped. Subject specific tissue probability maps for grey and white matter and cerebrospinal fluid were determined using a SPM based multichannel segmentation (SPM12, Welcome Trust Centre for Neuroimaging, University College, London, UK) using the 3D T1 BRAVO and T2 CUBE FLAIR.

Then, PET-MR data were spatially normalized to the MNI template using 3D T1 BRAVO and 3 tissue probability maps normalization (PMOD) and restricted to the subject-specific grey matter part of the whole brain with a fixed threshold of 0.3 (only voxel inclusion with high probability of belonging to grey matter). The tissue volume of distribution (V_T) was calculated using a 1- and 2-tissue compartment model (1-2TCM) and Logan graphical analysis (LGA) (PMOD v3.7) with blood volume fixed to 5% and equilibration time (t*) to 36 minutes. The most appropriate kinetic model was selected using the Akaike Information Criteria (AIC).

Next, this model was used to evaluate time stability of the PET acquisition time and the TRV of V_T. TRV was calculated as $2 \times \left(V_{T,i}^{test} - V_{T,i}^{retest}\right) / \left(V_{T,i}^{test} + V_{T,i}^{retest}\right)$ as well as in an absolute way (aTRV) as $2 \times \left|V_{T,i}^{test} - V_{T,i}^{retest}\right| / \left(V_{T,i}^{test} + V_{T,i}^{retest}\right)$, for each brain VOI.

Group comparisons were conducted at cluster level $p_{FWE\text{-}corr} < 0.05$, peak level $p_{height} < 0.001$, and a cluster extent threshold (k_e) of 50 voxels. V_T images were calculated and analysed using both individual and average metabolite corrected input curves to assess the robustness taking the late metabolite sample variability into account.

As no significant group atrophy effect was observed between PD and HV using a voxel-based morphometry analysis using CAT12 software in SPM (even at a lower threshold: cluster level $p_{uncorr} < 0.001$, peak level $p_{height} < 0.005$), PET analyses were performed without partial volume correction.

Genetics

The 13 exons of the P2X7R were all sequenced on venous samples (white blood cells) of the subjects of part 2. Genomic DNA was extracted using Chemagic DNA blood special 4 ml kit (Chemagen-Perkin Elmer, Baesweiler, Germany) on a Chemagen MSM automate (Chemagen-Perkin Elmer, Baesweiler, Germany). DNA purity was measured using a DropSense96 (Trinean, Belgium) with cDrop™ Software and DNA concentration using the Qubit ™ BR assay. From each sample, 10 µl DNA (10 ng/µl) was used for further analysis.

Molecular inversion probes (MIPs), containing end sequences complementary to the target DNA connected by a 30-base linker sequence, were designed, ordered and pooled at 100 µM [21]. After phosphorylation the MIP probes were added to the genomic DNA samples to capture the genomic regions of interest. Denaturation of the DNA was followed by hybridization of the probe ends to their complementary target sequence. Complementary bases were incorporated by a DNA polymerase in the gap between the 2 probe ends containing the genomic region of interest. The resulting DNA molecules were circularised by DNA ligase. Unbound linear probes and genomic DNA were removed by exonucleases. The captured regions of interest were barcoded and amplified in a PCR reaction. Using SPRI bead technology primer-dimers were removed. The samples were pooled at a concentration of 2nM. Sequencing was performed using paired-end sequencing on the Illumina MiSeq platform. Overlapping paired end reads were merged using flash2. Merged reads were mapped to the human genome (build hg19; bwa 0.7.5) prior to sorting by amplicon and variant calling per amplicon with GATK HaplotypeCaller (GATK 3.8). The positions in which at least one sample was polymorphic were used to genotype all samples together using GATK GenotypeGVCFs (GATK 3.8). Finally variants were annotated using Annovar (23-05-2015).

After genotyping, a relation between polymorphisms and V_T was sought. Therefore, we used the number of copies to create a percentage of variant allel to allow a correlation analysis, using the following formula: % variant allel = number of copies of variant allel / (number of copies variant allel + number of copies reference allel)

The percentage of variant copies therefore ranged from 0 (homozygote reference) to 1 (homozygote variant). A Spearman correlation coefficient was calculated using the percentage of variant allel and the composite cortical

V_T value – both using individual and average metabolite corrected input curves. In case a retest scan was conducted the average V_T value between test and retest was used.

General statistics

Conventional statistics were conducted in SPSS (version 24.0. Armonk, US) and significance was considered with p-value < 0.05 after Bonferroni correction for multiple comparisons.

RESULTS

Biodistribution and whole body dosimetry

Figure 1 shows coronal slices of the whole-body PET scan biodistribution data over time. The normalized TACs for brain, gallbladder, liver and intestines are shown in Figure 2. Predominantly hepatobiliary excretion was observed. In Supplementary Table 1, NCA for all source organs with significant activity uptake are listed with individual organ doses for all subjects with mean value and standard deviation. The organ absorbed doses were the largest for the gallbladder (25 µGy/MBq), the liver (22µGy/MBq) and the small intestine (20µGy/MBq). Average (± SD) value for ED was 4.47 ± 0.32 µSv/MBq (Supplementary Table 2), which is in the typical range for ^{11}C-radiolabelled ligands (5.7-1.2 µSv/MBq [22]).

Tracer kinetic modelling and test-retest variability

Model selection and intersubject variability assessment was performed on 10 PD patients and 11 HV (see Table 1). Fig 3 shows fitted TACs. AIC values were almost always (> 85%) lower for the 2TCM compared to 1TCM (Figure 3). Therefore, the 2TCM was selected as optimal model for [^{11}C]JNJ717 and reported results are restricted to the 2TCM V_T values.

Intersubject variability was acceptable with an average V_T of 3.4 ± 0.8 (range 2.0 – 6.7) for HV (CoV = 23.8 %) and an average V_T of 3.3 ± 0.7 (range 1.8 – 5.3) for PD patients (CoV = 21.7 %). Very similar results were obtained using the average metabolite curve (average V_T 3.2 ± 0.5 (range 2.4 – 4.6), for HV (CoV =15.0 %) and average V_T 3.2 ± 0.8 (range 1.5 – 4.7), for PD patients (CoV =23.5 %).

V_T was homogeneous across most cortical and subcortical brain regions (Figure 4 and 5), whereas the brainstem and striatum showed slightly higher mean [^{11}C]JNJ717 uptake (about 10%). Regarding time stability of V_T, we calculated the impact of reducing acquisition time to 60, 70 and 80 minutes, compared to the full 90 minute acquisition. Results are shown in Table 2 and Figure 6 , resulting in an acceptable average bias of around 5% (average 6.9 ± 8.3 for 2TCM and average 4.6 ± 4.1 for LGA [individual metabolite corrected input curve] , average 3.9 ± 3.7 for 2TCM and average 3.7 ± 3.7 for LGA [average metabolite corrected input curve]) for an acquisition time of 70 minutes. Reduction to 60 minutes lead to individual biases of more than 25 % both in cortical and subcortical regions.

TRV was calculated using a 90 minutes acquisition time for 2TCM and LGA. Results are shown in Table 3 for various subcortical and cortical brain regions. Average TRV and aTRV was - 4.7 % and 12.6 % using individual metabolite curves, respectively, and did not improve as values of - 7.7 % and 10.2 % using an average metabolite

curve, respectively, were found. In 2 subjects values were higher (30 - 40%), likely due to the high variation in test-retest metabolite fraction.

[^{11}C]-JNJ717 distribution volume in PD patients versus healthy controls

No absolute nor relative significant differences in [^{11}C]JNJ717 distribution volume were observed between PD and HV nor VOI- or voxel-based. Individual or average metabolite correction input curves did not change the results.

Genotyping

In total, 7 single nucleotide polymorphisms (SNP's) in the 13 exons of the P2X7R were identified of which 6 non-synonymous and 1 synonymous mutation (see Table 4). In 2 PD patients a lower V_T value (around 2 compared to around 3-5) was observed (Figure 5). One of these patients was homozygote for the variant rs3751143 while the other – although heterozygote - had a much higher number of copies of the variant allele in contrast to the other heterozygote subjects.

Additionally, the spearman correlation coefficient between the 7 SNP's and the V_T of the composite cortical VOI was calculated. Of these 7, only the reference SNP (rs) rs3751143 on exon 13 was significant after Bonferroni correction ($p_{spearman}$ = 0-0.60, p = 0.03) using individual metabolite corrected input curves (Figure 7A.). This correlation remained significant after using the V_T values calculated with the average metabolite corrected input curves ($p_{spearman}$ = -0.70, $p < 0.01$). (Figure 7B.)

DISCUSSION

[^{11}C]JNJ717 is a promising ligand to study P2X7R in vivo in the brain using PET imaging. It has, aside from its shorter half-life ^{11}C label allowing single-day multiple scanning, similar characteristics as its ^{18}F-analog [^{18}F]JNJ64413739 that was recently reported [20, 23]. Aside from these two clinically studied radioligands, several others have been developed and described in preclinical models with variable results [24-32].

The biodistribution of [^{11}C]JNJ717 showed moderate uptake in the brain (up to 5% of the injected dose), predominantly hepatobiliary clearance and a typical carbon-11 tracer effective dose (4.5 µSv/MBq) [22].

Similarly to the [^{18}F]JNJ64413739 compound, a reversible 2TCM model was able to fit [^{11}C]JNJ717 dynamic PET data reliably and distribution volume maps can be generated using a Logan graphical analysis (LGA) [20]. Relatively homogeneous uptake in grey matter was observed with an acceptable TRV of around 10-15%, again comparable to [^{18}F]JNJ64413739[20]. However, in contrast to [^{18}F]JNJ64413739 [20], acquisition time could be reduced to 70 minutes with an acceptable average bias of 5%.

This is the first time a microglial membrane bound neuroinflammation marker other than Translocator protein receptor (TSPOR) has been studied in PD with PET. TSPOR and P2X7R, are upregulated on activated microglia [33]. Nevertheless, P2X7R ligands may allow more specific early detection as P2X7R drives microglial activation [5]. In this study no significant differences in P2X7R expression and distribution between PD patients and HV were observed. Previously, a study with the TSPO ligand [^{11}C]DPA713 found a significantly higher BP_{nd} (10% to 25% increase) in the occipital, temporal and parietal regions in PD compared to controls [34]. Similarly, microglial activation has been observed in the pons, basal ganglia and frontal and temporal regions in PD using [^{11}C]PK11195 [35, 36]. Furthermore, Ouchi et al. demonstrated parallel changes in midbrain microglial activation with dopaminergic terminal loss in the putamen [37]. Additionally, treatment with AZD3241, a myeloperoxidase inhibitor, reduced nigrostriatal [^{11}C]PBR28 binding with around 15% in PD patients [38]. On the other hand, three other previous studies in PD using [^{18}F]FEPPA [39, 40] and [^{11}C]PK11195 [41] found no significant differences. Although results in the latter [^{11}C]PK11195 study were not significant, the authors described a trend towards increased microglial activation in the putamen and midbrain. Differences in patient populations with small sample sizes and tracer characteristics may play a role (e.g. [^{11}C]PK11195 has a low signal-to-noise-ratio) [42, 43]. Preclinical data have shown that pharmacological blockade of P2X7R is advantageous to reverse/diminish symptomatology in PD animal models [8, 11]. Moreover, gene expression analysis showed a small (two fold) increase of the P2X7R gene on RNA extracted

from the substantia nigra in PD patients [44]. Altogether, this provides only limited evidence for upregulation of P2X7R in PD [44]. Altered receptor function of P2X7 (e.g. more time in pore formation status) without change in expression levels might also explain the neuroprotective effect of P2X7R antagonism in pharmacological preclinical PD studies. On the other hand, radiotracer affinity compared to the level of P2X7R overexpression may be insufficient to detect subtle group differences, but it is unknown what the expression level is for P2X7R under chronic neuroinflammatory conditions in vivo. Possibly, as P2X7R is believed to orchestrate early microglial activation, P2X7R expression may be higher in prodromal PD patients. Recently, the involvement of P2X7R in early activation has been observed in a rat model of neuroinflammation using the ^{18}F-analog [^{18}F]JNJ64413739 where highest signal was observed two to three days after LPS injection after which this effect disappeared. Moreover, in this study increased uptake of [^{18}F]JNJ64413739 was shown to correspond with increased Iba1 staining, a microglial marker, thereby illustrating P2X7R radioligands likely visualize microglial activation [23]. P2X7R function may vary in time - illustrated in an ALS mice model and a neuroinflammation rat model- so upregulation may also be transient during the course of neurodegenerative diseases [12, 23]. Therefore, studies in prodromal patients and at different disease stages are needed to unravel P2X7R distribution during disease. Alternatively, as microglial activation in PD may be relatively limited compared to multiple system atrophy (MSA) [45], future studies in other neurodegenerative diseases such as MSA may provide additional insights. The latter has been supported by the consistent finding of increased microglial activation in atypical parkinsonian syndromes [46-50].

In this study 7 SNP's were observed in our subjects. Of these 7, only 1 (rs3751143) was significantly correlated with the composite cortical V_T, illustrated in Figure 7. Moreover, the significance remained after accounting for the metabolite variation, illustrating the stability of this finding. Genotyping is required for TSPO tracers as the rs6971 polymorphism divides the population in high, mixed and low affinity binders. Our observation could provide preliminary evidence for a similar genotype effect for [^{11}C]JNJ717 binding affinity or may reflect differences in expression level. The rs3751143 polymorphism is known to cause a loss of P2X7R function in normal conditions [51], demonstrating its functional importance. Although, the latter reported a low frequency of 2% for a homozygous substitution and 20% for a heterozygous substitution, this may impact sample size effect. Therefore, in future studies the rs3751143 should be investigated to confirm / reject this genotype effect. Considerable variation in microglial activation across PD patients has been observed in previous research which will be amplified by genotype effects. Therefore, a genotype effect could partly explain the lack of increased P2X7R binding in this group comparison.

This study has some limitations. Firstly, all PD patients were scanned on medication to facilitate a 90 minute scanning time because defining the optimal kinetic model was the principal aim of the study. However, no interaction between dopaminomimetics and P2X7R binding is to be expected. Also, in a Schizophrenia mouse model P2X7R depletion did not change the downregulation of D2 receptors and [^{3}H]dopamine release [52]. Secondly, because of high observed standard errors for the two last metabolite data points, all analyses were performed using both an individual and average metabolite fit, but very similar results were obtained, indicating the robustness of results despite this higher variability in metabolite correction curve.

CONCLUSION

[^{11}C]JNJ717 is a promising PET radioligand for quantifying P2X7R expression with sufficient brain uptake and a TRV of 10-15% using a reversible 2TCM. Acquisition time can be reduced to 70 minutes facilitating patient comfort. Additionally, a possible genotype effect was identified in rs3751143 (exon 13) which may cause differences in binding affinity or expression level. In a first pilot study in PD, no group differences in [^{11}C]JNJ717 uptake were found compared with HV on a voxel level. However, this radioligand can still be valuable in neurodegenerative and inflammatory diseases to answer valuable questions about disease pathogenesis, neuroinflammation, microglial activation and prognosis.

REFERENCES

1. Skaper SD, Facci L, Zusso M, Giusti P. An Inflammation-Centric View of Neurological Disease: Beyond the Neuron. Front Cell Neurosci. 2018;12:72.

2. Able SL, Fish RL, Bye H, Booth L, Logan YR, Nathaniel C et al. Receptor localization, native tissue binding and ex vivo occupancy for centrally penetrant P2X7 antagonists in the rat. Br J Pharmacol. 2011;162(2):405-14.

3. Bhattacharya A, Biber K. The microglial ATP-gated ion channel P2X7 as a CNS drug target. Glia. 2016;64(10):1772-87.

4. Masuch A, Shieh CH, van Rooijen N, van Calker D, Biber K. Mechanism of microglia neuroprotection: Involvement of P2X7, TNFalpha, and valproic acid. Glia. 2016;64(1):76-89.

5. Monif M, Burnstock G, Williams DA. Microglia: proliferation and activation driven by the P2X7 receptor. Int J Biochem Cell Biol. 2010;42(11):1753-6.

6. Chen X, Hu J, Jiang L, Xu S, Zheng B, Wang C et al. Brilliant Blue G improves cognition in an animal model of Alzheimer's disease and inhibits amyloid-beta-induced loss of filopodia and dendrite spines in hippocampal neurons. Neuroscience. 2014;279:94-101.

7. Diaz-Hernandez JI, Gomez-Villafuertes R, Leon-Otegui M, Hontecillas-Prieto L, Del Puerto A, Trejo JL et al. In vivo P2X7 inhibition reduces amyloid plaques in Alzheimer's disease through GSK3beta and secretases. Neurobiol Aging. 2012;33(8):1816-28.

8. Ferrazoli EG, de Souza HD, Nascimento IC, Oliveira-Giacomelli A, Schwindt TT, Britto LR et al. Brilliant Blue G, But Not Fenofibrate, Treatment Reverts Hemiparkinsonian Behavior and Restores Dopamine Levels in an Animal Model of Parkinson's Disease. Cell Transplant. 2017;26(4):669-77.

9. Wang XH, Xie X, Luo XG, Shang H, He ZY. Inhibiting purinergic P2X7 receptors with the antagonist brilliant blue G is neuroprotective in an intranigral lipopolysaccharide animal model of Parkinson's disease. Mol Med Rep. 2017;15(2):768-76.

10. Sluyter R, Bartlett R, Ly D, Yerbury JJ. P2X7 receptor antagonism in amyotrophic lateral sclerosis. Neural Regen Res. 2017;12(5):749-50.

11. Hracsko Z, Baranyi M, Csolle C, Goloncser F, Madarasz E, Kittel A et al. Lack of neuroprotection in the absence of P2X7 receptors in toxin-induced animal models of Parkinson's disease. Mol Neurodegener. 2011;6:28.

12. Apolloni S, Amadio S, Montilli C, Volonte C, D'Ambrosi N. Ablation of P2X7 receptor exacerbates gliosis and motoneuron death in the SOD1-G93A mouse model of amyotrophic lateral sclerosis. Hum Mol Genet. 2013;22(20):4102-16.

13. Yiangou Y, Facer P, Durrenberger P, Chessell IP, Naylor A, Bountra C et al. COX-2, CB2 and P2X7-immunoreactivities are increased in activated microglial cells/macrophages of multiple sclerosis and amyotrophic lateral sclerosis spinal cord. BMC Neurol. 2006;6:12.

14. Ory D, Celen S, Gijsbers R, Van Den Haute C, Postnov A, Koole M et al. Preclinical Evaluation of a P2X7 Receptor-Selective Radiotracer: PET Studies in a Rat Model with Local Overexpression of the Human P2X7 Receptor and in Nonhuman Primates. J Nucl Med. 2016;57(9):1436-41.

15. Fuller SJ, Stokes L, Skarratt KK, Gu BJ, Wiley JS. Genetics of the P2X7 receptor and human disease. Purinergic Signal. 2009;5(2):257-62.

16. Tomlinson CL, Stowe R, Patel S, Rick C, Gray R, Clarke CE. Systematic review of levodopa dose equivalency reporting in Parkinson's disease. Mov Disord. 2010;25(15):2649-53.

17. Stabin MG, Sparks RB, Crowe E. OLINDA/EXM: the second-generation personal computer software for internal dose assessment in nuclear medicine. J Nucl Med. 2005;46(6):1023-7.

18. Johansson L, Mattsson S, Nosslin B, Leide-Svegborn S. Effective dose from radiopharmaceuticals. Eur J Nucl Med. 1992;19(11):933-8.

19. Georg Schramm MK, Stefanie M. A. Willekens, Ahmadreza Rezaei, Donatienne Van Weehaeghe, Gaspar Delso, Ronald Peeters, Nathalie Mertens, Johan Nuyts, Koen Van Laere. Regional accuracy of ZTE-based attenuation correction in static and dynamic brain PET/MR. Medical Physics. 2018.

20. Koole M, Schmidt M, Hijzen A, Ravenstijn P, Vandermeulen C, Van Weehaeghe D et al. (18)F-JNJ-64413739, a novel PET ligand for the P2X7 ion channel: radiation dosimetry, kinetic modeling, test-retest variability and occupancy of the P2X7 antagonist JNJ-54175446. J Nucl Med. 2018.
21. Neveling K, Mensenkamp AR, Derks R, Kwint M, Ouchene H, Steehouwer M et al. BRCA Testing by Single-Molecule Molecular Inversion Probes. Clin Chem. 2017;63(2):503-12.
22. Zanotti-Fregonara P, Innis RB. Suggested pathway to assess radiation safety of 11C-labeled PET tracers for first-in-human studies. Eur J Nucl Med Mol Imaging. 2012;39(3):544-7.
23. Berdyyeva T, Xia C, Taylor N, He Y, Chen G, Huang C et al. PET Imaging of the P2X7 Ion Channel with a Novel Tracer [(18)F]JNJ-64413739 in a Rat Model of Neuroinflammation. Mol Imaging Biol. 2019.
24. Fantoni ER, Dal Ben D, Falzoni S, Di Virgilio F, Lovestone S, Gee A. Design, synthesis and evaluation in an LPS rodent model of neuroinflammation of a novel (18)F-labelled PET tracer targeting P2X7. EJNMMI Res. 2017;7(1):31.
25. Gao M, Wang M, Glick-Wilson BE, Meyer JA, Peters JS, Territo PR et al. Synthesis and initial in vitro characterization of a new P2X7R radioligand [(18)F]IUR-1602. Appl Radiat Isot. 2018;144:10-8.
26. Han J, Liu H, Liu C, Jin H, Perlmutter JS, Egan TM et al. Pharmacologic characterizations of a P2X7 receptor-specific radioligand, [11C]GSK1482160 for neuroinflammatory response. Nucl Med Commun. 2017;38(5):372-82.
27. Janssen B, Vugts DJ, Funke U, Spaans A, Schuit RC, Kooijman E et al. Synthesis and initial preclinical evaluation of the P2X7 receptor antagonist [(1)(1)C]A-740003 as a novel tracer of neuroinflammation. J Labelled Comp Radiopharm. 2014;57(8):509-16.
28. Janssen B, Vugts DJ, Wilkinson SM, Ory D, Chalon S, Hoozemans JJM et al. Identification of the allosteric P2X7 receptor antagonist [(11)C]SMW139 as a PET tracer of microglial activation. Sci Rep. 2018;8(1):6580.
29. Gao M, Wang M, Glick-Wilson BE, Meyer JA, Peters JS, Territo PR et al. Synthesis and preliminary biological evaluation of a novel P2X7R radioligand [(18)F]IUR-1601. Bioorg Med Chem Lett. 2018;28(9):1603-9.
30. Gao M, Wang M, Green MA, Hutchins GD, Zheng QH. Synthesis of [(11)C]GSK1482160 as a new PET agent for targeting P2X(7) receptor. Bioorg Med Chem Lett. 2015;25(9):1965-70.
31. Jin H, Han J, Resing D, Liu H, Yue X, Miller RL et al. Synthesis and in vitro characterization of a P2X7 radioligand [(123)I]TZ6019 and its response to neuroinflammation in a mouse model of Alzheimer disease. Eur J Pharmacol. 2018;820:8-17.
32. Territo PR, Meyer JA, Peters JS, Riley AA, McCarthy BP, Gao M et al. Characterization of (11)C-GSK1482160 for Targeting the P2X7 Receptor as a Biomarker for Neuroinflammation. J Nucl Med. 2017;58(3):458-65.
33. Tronel C, Largeau B, Santiago Ribeiro MJ, Guilloteau D, Dupont AC, Arlicot N. Molecular Targets for PET Imaging of Activated Microglia: The Current Situation and Future Expectations. Int J Mol Sci. 2017;18(4).
34. Terada T, Yokokura M, Yoshikawa E, Futatsubashi M, Kono S, Konishi T et al. Extrastriatal spreading of microglial activation in Parkinson's disease: a positron emission tomography study. Ann Nucl Med. 2016;30(8):579-87.
35. Gerhard A, Pavese N, Hotton G, Turkheimer F, Es M, Hammers A et al. In vivo imaging of microglial activation with [11C](R)-PK11195 PET in idiopathic Parkinson's disease. Neurobiol Dis. 2006;21(2):404-12.
36. Kobylecki C, Counsell SJ, Cabanel N, Wachter T, Turkheimer FE, Eggert K et al. Diffusion-weighted imaging and its relationship to microglial activation in parkinsonian syndromes. Parkinsonism Relat Disord. 2013;19(5):527-32.
37. Ouchi Y, Yoshikawa E, Sekine Y, Futatsubashi M, Kanno T, Ogusu T et al. Microglial activation and dopamine terminal loss in early Parkinson's disease. Ann Neurol. 2005;57(2):168-75.
38. Jucaite A, Svenningsson P, Rinne JO, Cselenyi Z, Varnas K, Johnstrom P et al. Effect of the myeloperoxidase inhibitor AZD3241 on microglia: a PET study in Parkinson's disease. Brain. 2015;138(Pt 9):2687-700.

39. Ghadery C, Koshimori Y, Coakeley S, Harris M, Rusjan P, Kim J et al. Microglial activation in Parkinson's disease using [(18)F]-FEPPA. J Neuroinflammation. 2017;14(1):8.
40. Koshimori Y, Ko JH, Mizrahi R, Rusjan P, Mabrouk R, Jacobs MF et al. Imaging Striatal Microglial Activation in Patients with Parkinson's Disease. PLoS One. 2015;10(9):e0138721.
41. Bartels AL, Willemsen AT, Doorduin J, de Vries EF, Dierckx RA, Leenders KL. [11C]-PK11195 PET: quantification of neuroinflammation and a monitor of anti-inflammatory treatment in Parkinson's disease? Parkinsonism Relat Disord. 2010;16(1):57-9.
42. Thobois S, Guillouet S, Broussolle E. Contributions of PET and SPECT to the understanding of the pathophysiology of Parkinson's disease. Neurophysiol Clin. 2001;31(5):321-40.
43. Firbank MJ, Yarnall AJ, Lawson RA, Duncan GW, Khoo TK, Petrides GS et al. Cerebral glucose metabolism and cognition in newly diagnosed Parkinson's disease: ICICLE-PD study. J Neurol Neurosurg Psychiatry. 2017;88(4):310-6.
44. Durrenberger PF, Grunblatt E, Fernando FS, Monoranu CM, Evans J, Riederer P et al. Inflammatory Pathways in Parkinson's Disease; A BNE Microarray Study. Parkinsons Dis. 2012;2012:214714.
45. Lim S, Chun Y, Lee JS, Lee SJ. Neuroinflammation in Synucleinopathies. Brain Pathol. 2016;26(3):404-9.
46. Dodel R, Spottke A, Gerhard A, Reuss A, Reinecker S, Schimke N et al. Minocycline 1-year therapy in multiple-system-atrophy: effect on clinical symptoms and [(11)C] (R)-PK11195 PET (MEMSA-trial). Mov Disord. 2010;25(1):97-107.
47. Gerhard A, Banati RB, Goerres GB, Cagnin A, Myers R, Gunn RN et al. [11C](R)-PK11195 PET imaging of microglial activation in multiple system atrophy. Neurology. 2003;61(5):686-9.
48. Gerhard A, Trender-Gerhard I, Turkheimer F, Quinn NP, Bhatia KP, Brooks DJ. In vivo imaging of microglial activation with [11C](R)-PK11195 PET in progressive supranuclear palsy. Mov Disord. 2006;21(1):89-93.
49. Gerhard A, Watts J, Trender-Gerhard I, Turkheimer F, Banati RB, Bhatia K et al. In vivo imaging of microglial activation with [11C](R)-PK11195 PET in corticobasal degeneration. Mov Disord. 2004;19(10):1221-6.
50. Passamonti L, Rodriguez PV, Hong YT, Allinson KSJ, Bevan-Jones WR, Williamson D et al. [(11)C]PK11195 binding in Alzheimer disease and progressive supranuclear palsy. Neurology. 2018;90(22):e1989-e96.
51. Gu BJ, Zhang W, Worthington RA, Sluyter R, Dao-Ung P, Petrou S et al. A Glu-496 to Ala polymorphism leads to loss of function of the human P2X7 receptor. J Biol Chem. 2001;276(14):11135-42.
52. Kovanyi B, Csolle C, Calovi S, Hanuska A, Kato E, Koles L et al. The role of P2X7 receptors in a rodent PCP-induced schizophrenia model. Sci Rep. 2016;6:36680.

Table 1: Demographics

	Disease status	Sex	Age (y)	Weight (kg)	Dose (MBq) Test (retest)	Mass (ug) Test (retest)	Molar Activity (GBq/µmol) Test (retest)	UPDRS motor (H&Y)	LED
Part 1: dosimetry									
1	HV	F	27	70	129	0.2	226	-	
2	HV	F	32	63	228	2.2	45	-	
3	HV	M	30	74	210	1.6	56	-	
Part 2: Kinetic modelling, test-retest variability and group comparison									
1	HV	F	55	60	154	0.5	129	-	
2	HV	M	73	70	161 (314)	2.0 (3.1)	34 (42)	-	
3	HV	F	40	68	310 (230)	3.9 (3.1)	25 (42)	-	
4	HV	F	53	78	187 (280)	0.7 (0.7)	107 (179)	-	
5	HV	M	75	70	307 (258)	4.8 (0.9)	27 (119)	-	
6	HV	M	63	114	236	0.9	115	-	
7	HV	M	66	92	325	1.0	136	-	
8	HV	F	53	75	210	1.6	53	-	
9	HV	F	60	66	247	0.4	233	-	
10	HV	F	68	59	302	0.9	138	-	
11	HV	M	69	79	254	0.9	116	-	
12	PD	M	75	83	304	0.8	165	22 (1)	660
13	PD	M	46	85	134 (278)	1.3 (2.8)	44 (42)	13 (1)	615
14	PD	M	59	102	216	3.5	26	31 (2)	605
15	PD	M	62	80	279 (222)	4.2 (2.0)	28 (46)	11 (1)	505
16	PD	M	69	76	271 (211)	1.0 (0.6)	110 (211)	30 (2)	250
17	PD	F	60	63	153	1.2	54	13 (1)	400
18	PD	F	66	50	304	0.6	231	15 (1)	405
19	PD	F	65	65	228	0.4	218	19 (1)	205
20	PD	M	73	90	175	0.4	192	34 (2)	1840
21	PD	M	58	90	244	0.7	153	25 (2)	105

Table 2: Baseline 2TCM V_T using an acquisition time of 90, 80, 70 and 60 min and baseline LGA V_T using a 90, 80, 70 and 60 min acquisition time interval for different brain regions. Statistics are given as mean ± SD [range]. A. Using individual metabolite curves B. Using average metabolite curves

A.

	2TCM V_T (90 min)	**2TCM V_T (80 min)**	**2TCM V_T (70 min)**	**2TCM V_T (60 min)**	**LGA V_T (90 min)**	**LGA V_T (80 min)**	**LGA V_T (70 min)**	**LGA V_T (60 min)**
Composite Cortical	3.5 ± 0.8 [2.1-5.3]	3.3 ± 0.8 [2.0-4.9]	3.2 ± 0.7 [1.9-4.6]	3.1 ± 0.7 [1.8-4.4]	3.4 ± 0.7 [2.1-4.9]	3.3 ± 0.7 [2.0-4.7]	3.2 ± 0.7 [1.9-4.5]	3.1 ± 0.7 [1.9-4.3]
Frontal	3.4 ± 0.8 [2.1-5.4]	3.3 ± 0.8 [2.0-5.0]	3.2 ± 0.7 [1.9-4.6]	3.1 ± 0.7 [1.8-4.2]	3.4 ± 0.8 [2.0-4.9]	3.3 ± 0.7 [2.0-4.7]	3.2 ± 0.7 [1.9-4.5]	3.1 ± 0.7 [1.8-4.3]
Temporal	3.5 ± 0.8 [2.3-5.3]	3.4 ± 0.7 [2.1-4.9]	3.2 ± 0.7 [1.9-4.6]	3.1 ± 0.6 [1.8-4.5]	3.4 ± 0.7 [2.1-4.8]	3.3 ± 0.7 [2.0-4.7]	3.2 ± 0.7 [1.9-4.5]	3.1 ± 0.6 [1.9-4.3]
Parietal	3.5 ± 0.8 [2.2-5.4]	3.4 ± 0.8 [2.1-5.1]	3.3 ± 0.8 [1.9-4.9]	3.2 ± 0.7 [1.8-4.6]	3.4 ± 0.8 [2.1-4.9]	3.3 ± 0.7 [2.0-4.8]	3.2 ± 0.7 [1.9-4.6]	3.1 ± 0.7 [1.9-4.4]
Occipital	3.5 ± 0.7 [2.3-5.1]	3.4 ± 0.7 [2.2-4.7]	3.2 ± 0.7 [2.0-4.5]	3.1 ± 0.7 [1.9-4.6]	3.4 ± 0.7 [2.2-4.8]	3.3 ± 0.7 [2.1-4.6]	3.2 ± 0.7 [2.0-4.5]	3.2 ± 0.7 [1.9-4.4]
Cerebellum	3.1 ± 0.7 [2.0-4.5]	2.9 ± 0.6 [1.8-4.1]	2.8 ± 0.6 [1.7-3.9]	2.7 ± 0.5 [1.6-3.9]	2.9 ± 0.6 [1.8-4.1]	2.9 ± 0.6 [1.7-4.0]	2.8 ± 0.5 [1.6-3.9]	2.7 ± 0.5 [1.6-3.8]
Striatum	3.9 ± 1.0 [2.2-6.4]	3.7 ± 0.9 [2.0-5.4]	3.5 ± 0.8 [1.9-5.2]	3.4 ± 0.8 [1.9-4.9]	3.5 ± 0.8 [2.1-5.2]	3.5 ± 0.8 [2.0-5.2]	3.4 ± 0.7 [1.9-5.1]	3.3 ± 0.7 [1.9-4.7]
Corpus callosum	3.6 ± 1.0 [2.1-5.7]	3.4 ± 0.9 [2.0-5.6]	3.4 ± 0.9 [1.8-5.4]	3.3 ± 0.9 [1.8-5.2]	3.3 ± 0.8 [1.9-5.2]	3.2 ± 0.8 [1.9-5.0]	3.1 ± 0.7 [1.7-4.6]	3.0 ± 0.6 [1.7-4.1]

B.

	2TCM V_T (90 min)	2TCM V_T (80 min)	2TCM V_T (70 min)	2TCM V_T (60 min)	LGA V_T (90 min)	LGA V_T (80 min)	LGA V_T (70 min)	LGA V_T (60 min)
Composite Cortical	3.3 ± 0.7 [1.7-4.4]	3.2 ± 0.7 [1.7-4.4]	3.1 ± 0.7 [1.6-4.3]	3.1 ± 0.7 [1.6-4.3]	3.3 ± 0.7 [1.7-4.5]	3.2 ± 0.7 [1.7-4.5]	3.1 ± 0.7 [1.6-4.4]	3.1 ± 0.7 [1.6-4.3]
Frontal	3.2 ± 0.7 [1.7-4.6]	3.1 ± 0.7 [1.6-4.5]	3.1 ± 0.7 [1.6-4.5]	3.0 ± 0.7 [1.6-4.3]	3.3 ± 0.7 [1.7-4.6]	3.2 ± 0.7 [1.6-4.6]	3.1 ± 0.7 [1.6-4.6]	3.1 ± 0.7 [1.6-4.4]
Temporal	3.3 ± 0.7 [1.7-4.4]	3.2 ± 0.6 [1.7-4.3]	3.1 ± 0.7 [1.6-4.2]	3.0 ± 0.6 [1.6-4.2]	3.2 ± 0.6 [1.7-4.4]	3.2 ± 0.6 [1.7-4.3]	3.1 ± 0.6 [1.6-4.2]	3.0 ± 0.6 [1.6-4.1]
Parietal	3.3 ± 0.7 [1.7-4.8]	3.2 ± 0.7 [1.7-4.7]	3.2 ± 0.7 [1.6-4.6]	3.1 ± 0.7 [1.6-4.5]	3.3 ± 0.7 [1.7-4.7]	3.2 ± 0.7 [1.7-4.7]	3.2 ± 0.7 [1.7-4.6]	3.1 ± 0.7 [1.6-4.4]
Occipital	3.3 ± 0.7 [1.8-4.5]	3.2 ± 0.7 [1.7-4.5]	3.1 ± 0.7 [1.7-4.4]	3.1 ± 0.7 [1.6-4.4]	3.3 ± 0.7 [1.8-4.5]	3.2 ± 0.7 [1.7-4.5]	3.2 ± 0.7 [1.7-4.4]	3.1 ± 0.7 [1.6-4.4]
Cerebellum	2.8 ± 0.5 [1.5-3.7]	2.8 ± 0.5 [1.4-3.6]	2.7 ± 0.5 [1.4-3.6]	2.8 ± 0.6 [1.4-4.4]	2.8 ± 0.5 [1.5-3.7]	2.8 ± 0.5 [1.4-3.7]	2.7 ± 0.5 [1.4-3.6]	2.7 ± 0.5 [1.4-3.6]
Striatum	3.6 ± 1.0 [1.7-5.9]	3.5 ± 1.0 [1.7-6.1]	3.4 ± 0.8 [1.6-4.7]	3.3 ± 0.8 [1.6-4.7]	3.4 ± 0.8 [1.7-4.7]	3.4 ± 0.8 [1.7-4.8]	3.3 ± 0.8 [1.6-4.7]	3.3 ± 0.7 [1.6-4.5]
Corpus callosum	3.4 ± 1.0 [1.6-4.9]	3.4 ± 0.9 [1.6-4.9]	3.3 ± 0.9 [1.5-4.8]	3.3 ± 0.9 [1.5-5.0]	3.1 ± 0.8 [1.6-4.6]	3.0 ± 0.8 [1.5-4.5]	3.0 ± 0.7 [1.5-4.2]	2.9 ± 0.6 [1.4-3.9]

Table 3: Percentage test-retest variability using individual metabolite curves assessed as $2 \times (V_T^{test} - V_T^{retest})/(V_T^{test} + V_T^{retest})$ (TRV) and $2 \times |V_T^{test} - V_T^{retest}|/(V_T^{test} + V_T^{retest})$ (aTRV), averaged over the 7 test-retest datasets for different brain regions, together with the between-subject variability BS (%COV) of the average test-retest V_T across the 7 datasets. The intra-class correlation coefficient (ICC) is reported as measure for reliability and calculated as (BSMSS-WSMSS)/ (BSMSS+WSMSS) with BSMSS and WSMSS the mean sum of squares between subjects and within subjects, respectively.

	V_T (90 min) individual metabolite		**V_T (90 min) average metabolite**	
	TRV	**aTRV**	**TRV**	**aTRV**
Cortical	-4.7 [-35.1 - 32.0]	10.5 [0.0 – 36.9]	-7.7 [-29.5 – 9.1]	7.5 [0.3 – 30.6]
Frontal cortex	-3.9 [-34.4 - 23.7]	10.8 [0.0 – 34.4]	-7.0 [-28.1 – 6.5]	8.9 [2.9 – 28.1]
Temporal cortex	-4.3 [-35.6 - 32.1]	13.5 [0.0 – 35.6]	-8.3 [-28.8 – 8.5]	10.7 [2.8 – 28.8]
Parietal cortex	-4.7 [-35.8 - 26.2]	12.2 [0.0 – 35.8]	-8.0 [-30.8 – 7.7]	10.2 [2.8 – 30.8]
Occipital cortex	-4.0 [-34.3 - 31.2]	13.3 [0.0 – 34.3]	-7.7 [-32.1 – 12.5]	11.3 [2.4 – 32.1]
Cerebellum	-4.7 [-38.0 - 26.8]	12.8 [0.0 – 38.0]	-7.5 [-32.4 – 7.2]	9.6 [0.2 – 32.4]
Striatum	-5.9 [-36.9 - 16.6]	16.9 [0.0 – 43.8]	-6.8 [-30.6 – 2.2]	15.3 [10.8 – 21.7]
Thalamus	-5.5 [-40.6 - 21.2]	11.7 [0.0 – 40.6]	-7.7 [-29.5 – 9.1]	10.3 [2.4 – 35.2]

Table 4: Single nucleotide polymorphisms in the 13 exons of the P2X7R. (x, y) = x copies of ref and y copies of var; var = homozygote variant; ref = homozygote reference; htr = heterozygote; syn = synonymous single nucleotide variant.

	rs	ref	var	1	2	3	4	5	6	7	8	9	10	11	12	13	14	15	16	17	18	19	20	21
Exon 5	rs 208294	T	C	htr (282, 212)	htr (227, 224)	htr (231, 262)	var	htr (271, 234)	htr (257, 226)	ref	var	var	var	var	htr (289, 212)	htr (283, 217)	htr (229, 270)	htr (271, 228)	htr (82, 82)	var	htr (253, 247)	ref	var	ref
Exon 8	rs 7958311	G	A	htr (679, 746)	ref	htr (718, 787)	htr (811, 845)	htr (847, 923)	htr (571, 661)	htr (792, 763)	htr (681, 612)	htr (748, 888)	var	ref	htr (690, 629)	htr (780, 799)	ref	htr (787, 882)	ref	var	ref	ref	htr (751, 674)	var
Exon 8	rs7958316	G	A	ref	ref	ref	ref	ref	ref	ref	ref	ref	ref	ref	ref	ref	ref	ref	ref	ref	ref	ref	ref	htr (211, 206)
Exon 9	G920A	G	A	ref	ref	ref	ref	ref	ref	ref	ref	ref	htr (169, 221)	ref	ref	ref	ref	ref	ref	ref	ref	ref	ref	ref
Exon 11	rs 1718119	G	A	ref	htr (632, 790)	htr (768, 852)	ref	ref	ref	htr (598, 756)	htr (577,756)	htr (785, 719)	ref	htr (215, 314)	htr (614, 744)	ref	htr (670, 36)	ref	ref	ref	ref	htr (495, 762)	ref	ref
Exon 13	rs 3751143	A	C	htr (564, 555)	htr (442, 489)	ref	htr (463, 487)	htr (425, 455)	htr (371, 436)	ref	ref	ref	ref	ref	ref	htr (499, 504)	ref	htr (535, 523)	htr (205, 221)	ref	var	htr (286, 447)	ref	ref
Exon 13	syn, G1746A	G	A	ref	htr (319, 221)	htr (309, 343)	ref	ref	ref	htr (264, 295)	htr (345, 329)	htr (318, 313)	ref	htr (66, 19)	htr (251, 335)	ref	htr (305,264)	ref	ref	ref	ref	htr (130, 207)	ref	ref

Figure 1: Whole-body time-activity distribution [^{11}C]JNJ717 in subject number 1 (Table 1), with representative coronal slices. PET image colour intensities are relative to the maximum colour table values as indicated in the side row (SUV), in order to account for physical tracer decay. The lower row indicates the start (minutes) of the whole body scan. p.i. = postinjection

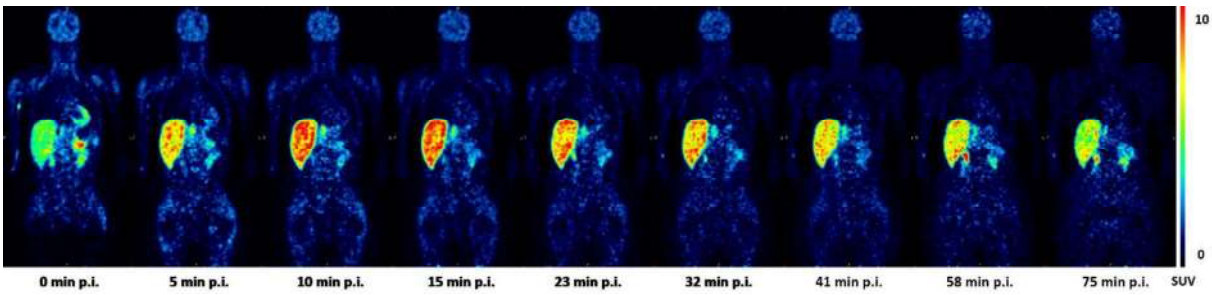

Figure 2: Mean fractional activity with respect to total body activity (circles, triangles and squares) with their respective curve fits (lines) for all subjects for brain, gallbladder, intestines and liver.

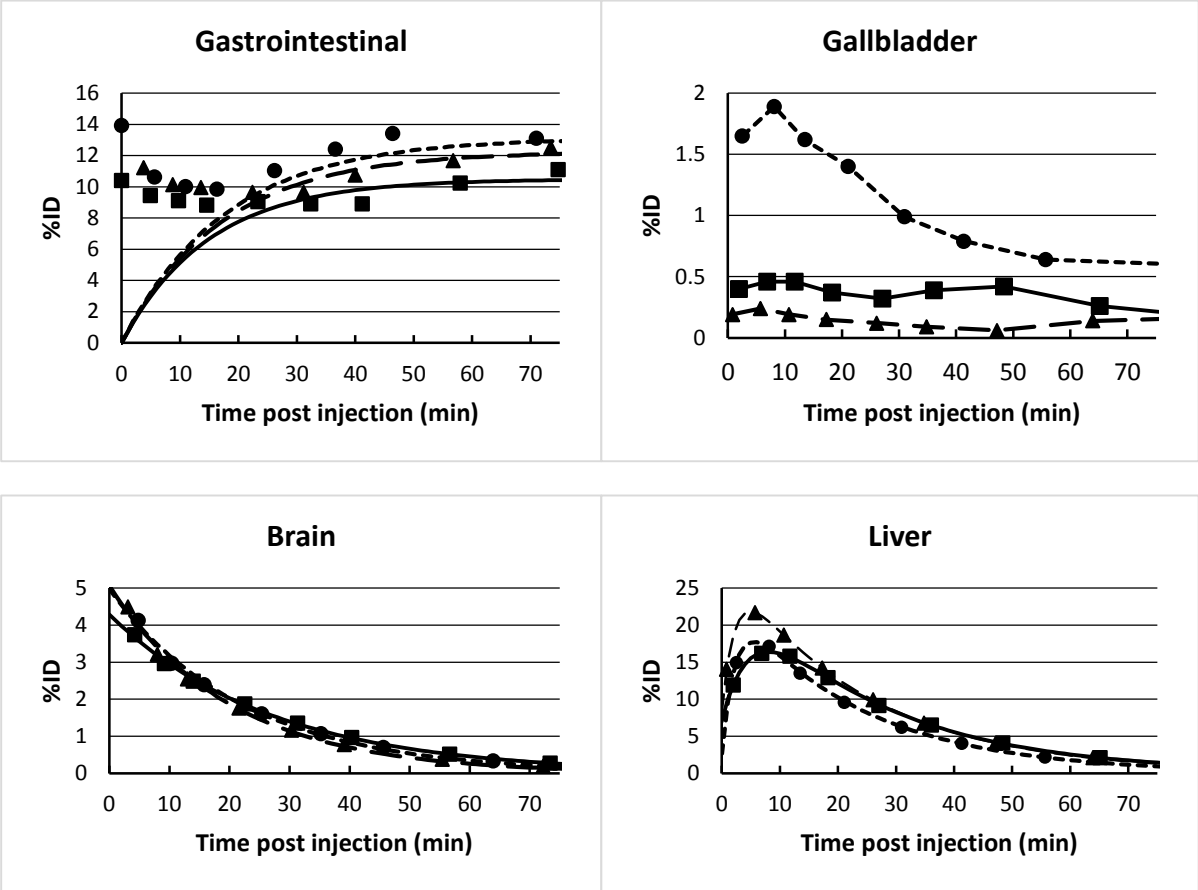

Figure 3: Representative 1TCM and 2TCM fits for a baseline composite cortical TAC and corresponding arterial blood/plasma input function (above). 1TCM and 2TCM AIC values for model fitting to baseline TACs of different brain regions of 10 PD and 11 HV (below).

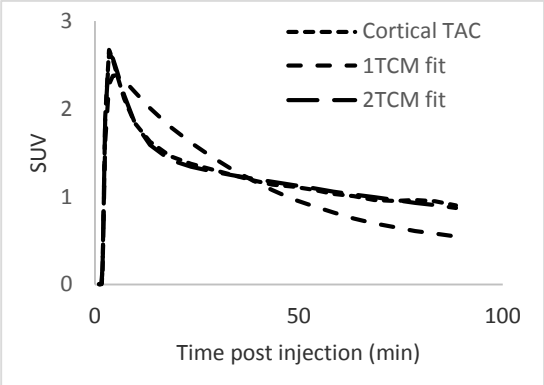

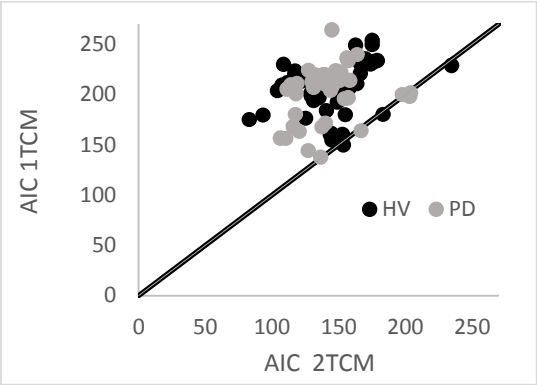

Figure 4: Average parametric LGA V_T images for healthy volunteers (HV) and Parkinson's disease (PD) patients.

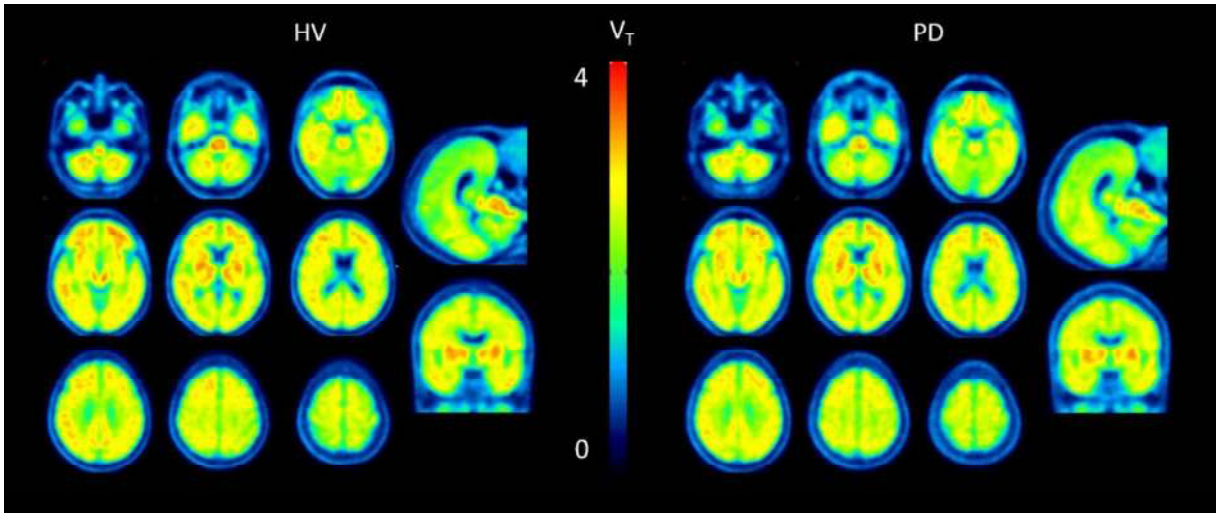

Figure 5: A. Overview of V_T values in Parkinson's Disease (PD) patients and healthy volunteers (HV) (test and retest combined) using individual metabolite curves. B. Overview of V_T values in PD and HV (test and retest combined) using average metabolite curves. C. Average metabolite curves with standard deviation in HV and PD.

A.

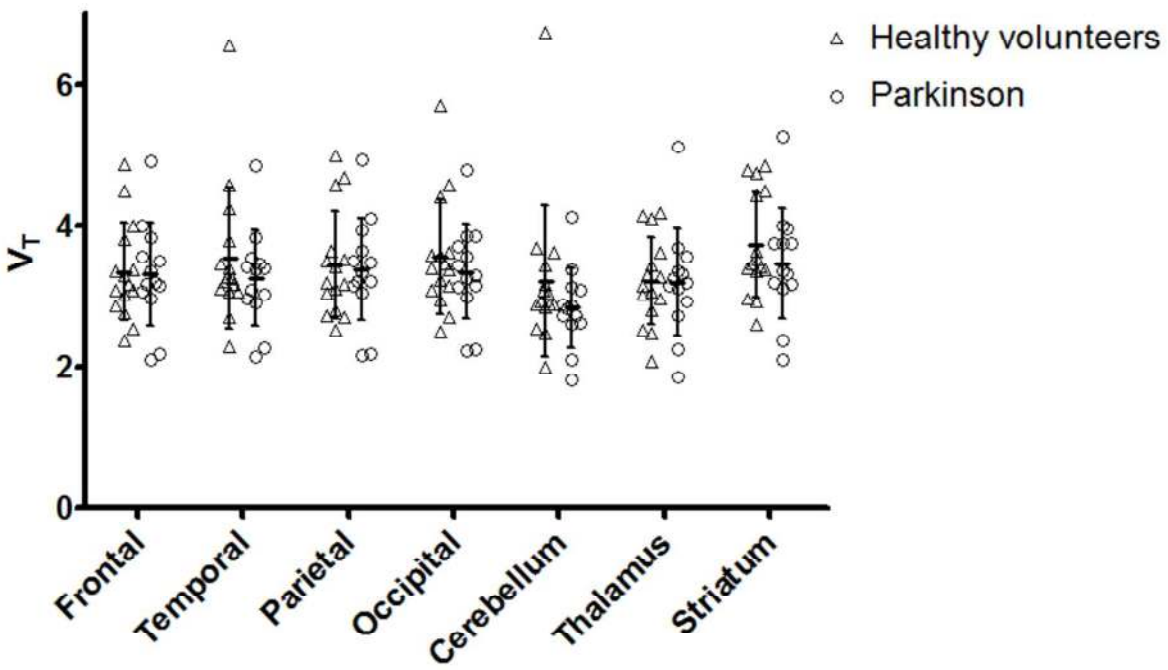

B.

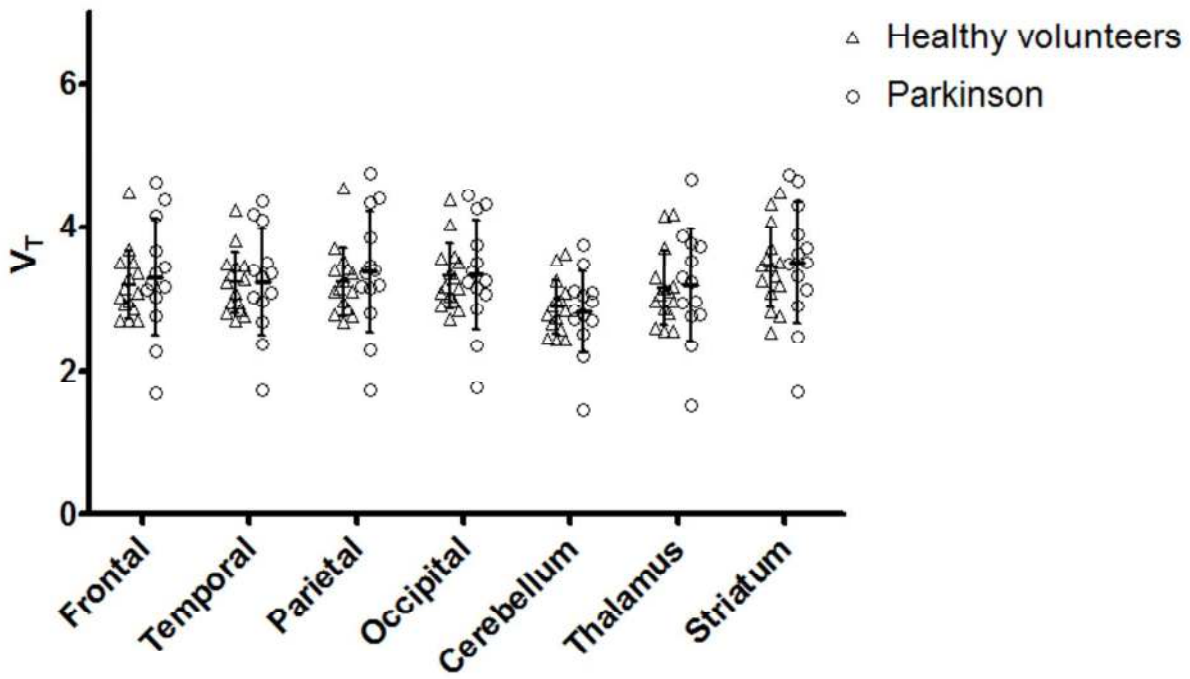
Healthy volunteers
Parkinson
V_T
0
2
4
6
Frontal
Temporal
Parietal
Occipital
Cerebellum
Thalamus
Striatum

C.

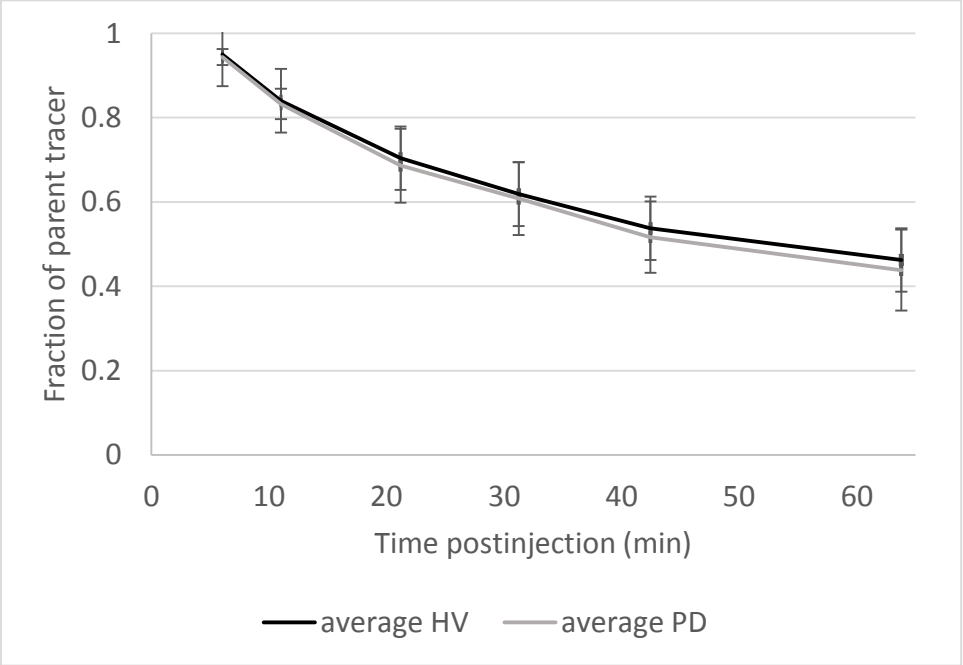
Fraction of parent tracer
0
0.2
0.4
0.6
0.8
1
0
10
20
30
40
50
60
Time postinjection (min)
average HV
average PD

Figure 6: Overview of percentage difference compared to the full 90-minutes time window with time reduction to 60 minutes in different cortical and subcortical regions.

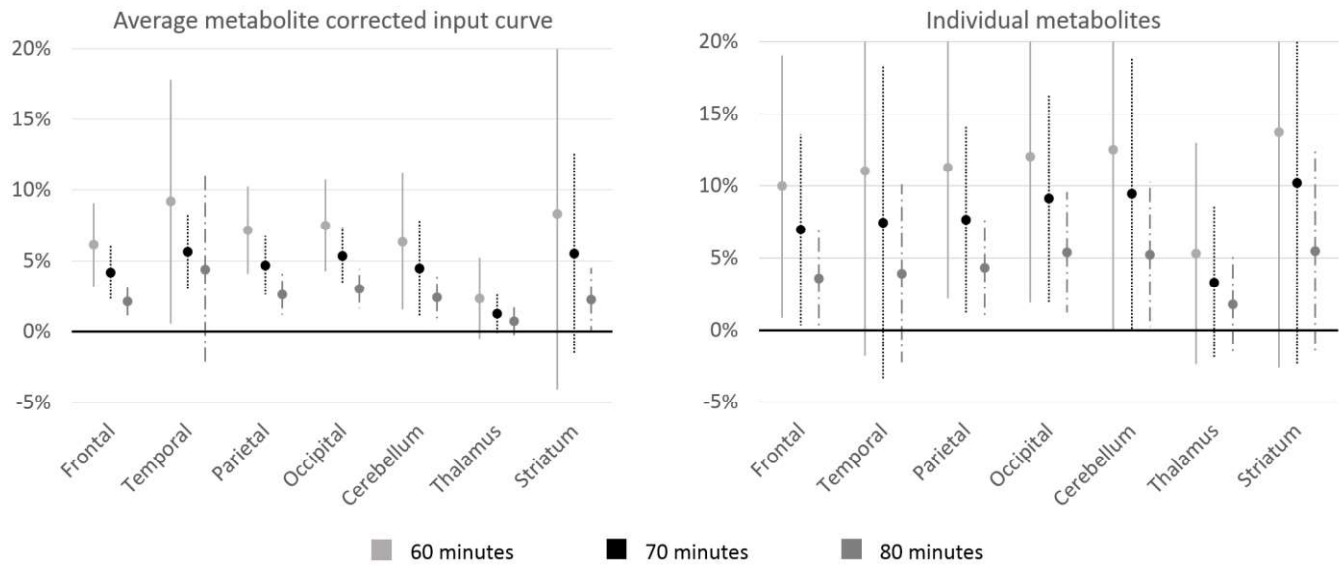

Figure 7: Correlation between rs3751143 and V_T of the composite cortical VOI with the 95% confidence interval (dashed line). A. Using the individual metabolite curves. B. Using the average metabolite curves.

A.

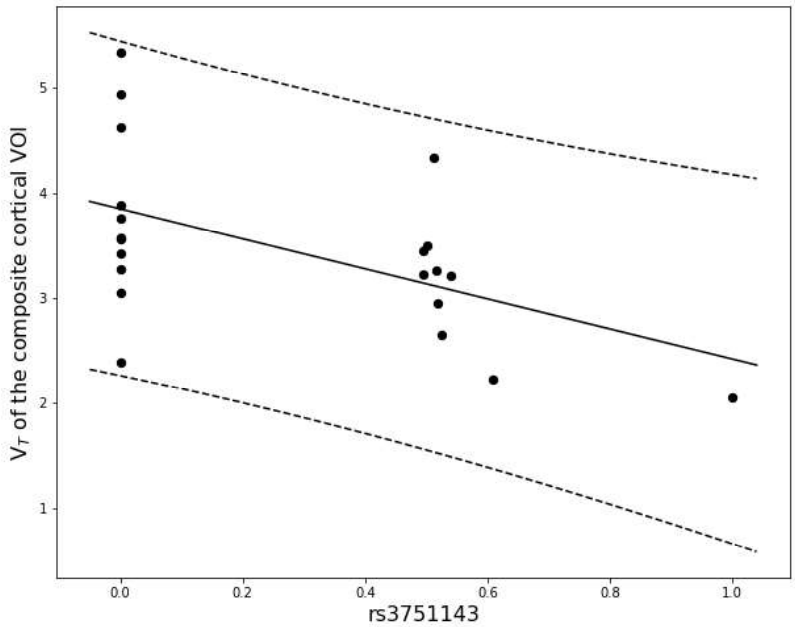

B.

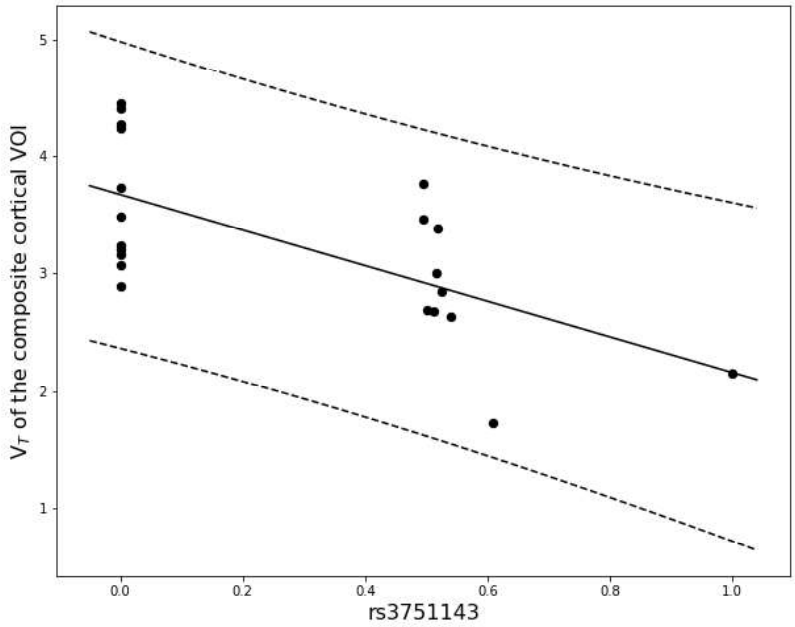

DISCLOSURES

The study was partially sponsored by a Michael J Fox Foundation Grant "PRI-PD" nr. #12062 and tracer development was partially sponsored by the EU FP7 project InMind. The precursor for the study was kindly donated by Janssen Pharmaceuticals. Koen Van Laere and Wim Vandenberghe are Senior Clinical Investigators of the Fund for Scientific Research, Flanders, Belgium (FWO). Donatienne Van Weehaeghe is a PhD fellow of the FWO. There are no other conflicts of interest.

COMPLIANCE WITH ETHICAL STANDARDS

Ethical approval: All procedures performed in studies involving human participants were in accordance with the ethical standards of the institutional and/or national research committee and with the 1964 Helsinki declaration and its later amendments or comparable ethical standards.

Informed consent: Written informed consent was obtained from all individual participants prior to their inclusion in the study.